Asian Journal of Chemistry; Vol. 37, No. 7 (2025), 1614-1628

ASIAN JOURNAL OF CHEMISTRY

https://doi.org/10.14233/ajchem.2025.33894

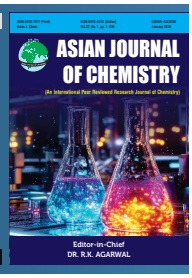

MD and DFT Studies of O–H···N Bonded Hordenine Dimer, Aided by Experimental Vibrational Spectroscopy, NBO, AIM and NCI Calculations

JYOTI BHOVI, J. TONANNAVAR and JAYASHREE J. TONANNAVAR*

Vibrational Spectroscopy/Molecular Modeling Laboratory, Department of Physics, Karnatak University, Dharwad-580003, India

*Corresponding author: E-mail: jjtonannavar@kud.ac.in

Received: 18 April 2025; *Accepted*: 29 May 2025; *Published online*: 30 June 2025; AJC-22035

The role of allelopathic and biochemical inhibitor hordenine in many applications may be determined by its potential tendency to the inter–molecular O–H···N bonding among other things. It is of interest to study multi-structural characterizations of the O–H···N bonding interaction to gain insights into the possible functional roles of the bonding, which may be correlated to the diverse application domains. In the present study, we have shown that the O–H···N bonded dimer computed from molecular dynamics (MD) simulation has short-range order and quasi-long range order consistent with the reported XRD results. We computed structural parameters from MD simulation in water yielding radius of gyration, minimum distance and root-mean-square-deviation and radial distribution function values that have been employed to understand the structural behaviour of the dimer. In addition, MD simulation also yielded O–H···O and C–H···N bonds as constituent links in dimer structures. We also combined molecular dynamics (MD) with DFT at B3LYP/6–311++G (d,p) level for computing the afore-mentioned stable structures and associated vibrational and electronic properties. Vibrational IR and Raman spectral features support the O–H···N bonded dimer structure. The orbitals overlap corresponding to the O–H···N bonding interaction has more contributions from s-orbitals of the O–H bond causing its elongation and stretching-mode red shift in the IR. The electron density and its Laplacian values have provided contour maps corresponding to the charge concentration and depletions around the O–H···N bond interaction.

Keywords: Hordenine, Molecular dynamics, DFT, O–H···N bond, Non-covalent interactions.

INTRODUCTION

Hordenine is a phenylethylamine (2-(4-hydroxyphenyl)-N,N-dimethylethylamine) alkaloid and is a natural compound found in barley, fungi and cacti. It is associated with many roles in pharmacology and human diseases from being allelopathic in plants to biochemical inhibitor in humans [1-7]. hordenine was first isolated from the sprouts of barley (*Hordeum vulgare*) from which it has derived its name. Other applications of hordenine include its usage as an ingredient in nutritional supplements and weight loss promoter [8]. It is apparent from its structure, Fig. 1, that hordenine, being the amphoteric due to the presence of both amine (NH_2, basic) and phenol (O–H, acidic) functional species, should engage itself in intermolecular bonds or non-covalent interactions. The biochemical processes entail such H-bond induced interactions for determining structural and functional outcomes among other things [9]. The presence of the hydroxyl moiety (–OH) in the *p*-position and 2–N$(CH_3)_2$ in ethyl moiety in the *meta*–position make hordenine molecule neutral. In neutral hordenine, the –OH moiety serves as the primary hydrogen bond donor, while the N–$(CH_3)_2$ group acts as the acceptor, leading to the formation of the O–H···N bond as has been shown in the reported XRD study [10]. The XRD structure comprises the head–to–tail arrangement as defined by O–H···N bonds. Furthermore, recent experimental investigations of hordenine with tyramine and N–methyl tyramine structures have shown that its monomer structure is stable due to the presence of C–H···N hyperconjugative interactions [11]. It is of vital importance to understand the role of the non-covalent interactions particularly O–H···N bond whose multi-fold characterization is amenable to the current computational tools, namely, density functional theory (DFT), classical molecular dynamics (MD), atoms-in-molecules (AIM) and non-covalent interactions (NCI). Observation of the vibrational IR modes of hordenine has shown the presence of O–H···N bond but far from being simple to analyze the vibrational structure due to the unresolved broad band contour near 3100 cm^{-1} extended down to 2500 cm^{-1}. Both XRD structure and IR band features

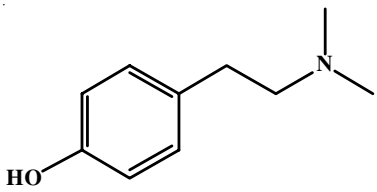

Fig. 1. Molecular structure of hordenine

strongly indicate hordenine being at least a dimer species bound principally by the O–H···N bond. Many times, a conventional interpretation of vibrational spectra is to assign away bands to the respective modes of the H-bonds without characterizing their intricate structural aspects.

In the present study, we propose to investigate the problem as follows: first, the most stable H-bonded dimer is found using molecular dynamics (MD) simulation since in the simulation process, a time-evolution of monomer species of hordenine into dimer species can be monitored through a pre-selected time window. This provides desired dimer species as time-averaged NCI structures as natural outcomes. This is the primary motive to prefer MD simulation to DFT calculations in finding dimer species. Second, the resultant dimer species are optimized to the most stable structure for further analysis. Third, the different MD structural characterizations so as to relate to vibrational and electronic properties are computed for gaining insights into the O–H···N bonded dimer structure.

To the best of our knowledge, no molecular dynamics (MD) simulation of O–H···N bonded hordenine dimer structure in a water solvent has been reported. Furthermore, it is of interest to understand how the O–H···N bond can be characterized using the radius of gyration (R_g), minimum distances between monomers in dimer species and root-mean-square-deviations (RMSD) of the trajectories of the atoms in the dimer configuration as a function of MD simulation run time yielding the idea of mobility. This defines a motivation for the present study. We have proposed the most stable dimer structure formed by an intermolecular O–H···N bond as determined by MD simulation and also consistent with the reported XRD structure. MD has also yielded intermolecular O–H···O bonded dimer species for hordenine. According to MD simulation, the hydroxyl–2(dimethylamino)-ethyl and hydroxyl–hydroxyl groups take part in the formation of O–H···N/O–H···O bonds in the dimer species. We have seen the transient O–H···N/O–H···O bonded dimer species with lifetimes of ~35 and 12 ps, respectively. Computed RDF which spatially determine O–H bond with respect to the N and O atoms, all lying within a spherical ring and as defined by the H–bond geometrical parameters, support the existence of H···N and H···O bonds in the dimer species. A broad IR absorption band profile with a number of embedded bands near 3110–2520 cm^{-1} provide the evidence of O–H···N bonded dimer with a red–shift in the IR stretching frequency of O–H bond by about ~16%. As complementary tool to IR, Raman band features satisfactorily support spectral analysis. Topological parameters like electron density, its Laplacian and other energetics computed from Bader's QTAIM–have been employed to characterize the strength of O–H···N bond [12]. Further, the O–H···N dimer structure including the weaker van der Waals interactions and steric clashes have also been evaluated by the 2D scatter plots and 3D isosurfaces using Johnson's NCI technique.

EXPERIMENTAL

Hordenine compound used was the solid powder sample ($C_{10}H_{15}NO$; m.w.: 165.23 g/mol; assay ~ 97%, Sigma–Aldrich, India). The absorption IR spectra (4000–400 cm^{-1}) were measured on a Thermo–Fisher Nicolet 6700 FT–IR spectrometer. The spectrometer had standard optical interferometry with Globar IR source and DTGS detector. Sampling method was based on the pellet technique: the pellets were made from the sample mixed with KBr in a 1:100 ratio and the IR spectra were recorded with 4 cm^{-1} resolution for 100 scans. The Raman spectra in the range 4000–50 cm^{-1} were measured on a Bruker RFS27 stand–alone FT–Raman spectrometer module equipped with an Nd:YAG laser source providing 1064 nm as the exciting line. A LN_2 cooled–Ge detector in the spectrometer system collected the Raman signals 500 scans at a resolution of 2 cm^{-1}. These parameters ensured the optimum Raman spectrum showing weak bands also.

Computational techniques

Determination of stable monomer structure: As a first step in finding the most stable monomer and dimer structures, we used alternately DFT and MD simulations. All the DFT calculations were run using Gaussian 09W suite [13] and Gromacs 5.1.1 package [14] on a dedicated Workstation. The dihedral angle between the phenol ring and the substituent (dimethylaminoethyl) moiety was varied in increments of 10º for the scan coordinates from 0 to 360º yielding the potential energy surface (PES) result at B3LYP/3–21G level (Fig. 2). The B3LYP/3–21G despite being lower level saved computational cost and in so far as our experience goes, it is satisfactorily reliable for the purpose of calculating PES. Four minimum energy monomers, say, M1, M2, M3 and M4, were obtained (Table-1). The most stable monomer M4 was selected for which we ran the classical MD simulations.

TABLE-1
GIBBS FREE ENERGIES, RELATIVE ENERGIES AND BOLTZMANN POPULATIONS FOR THE MINIMUM STRUCTURES OF HORDENINE MOLECULE

Minimum structures	Gibbs free energy G (Hartree)	Relative energy ΔG (kcal/mol)	Population (%)
Structure M1	-513.83667302	0.00005135	24.33
Structure M2	-513.83668402	0.00004035	25.38
Structure M3	-513.83671386	0.00001051	24.60
Structure M4	-513.83672437	0.00000000	25.67

MD and DFT computations: A detailed classical MD simulation procedure has been described earlier [15]. However, we describe the most essential steps adopted in the simulation. Before we ran MD simulations, the M4 was optimized at B3LYP/6–311++G(d,p) level producing M′4 and it still remains the lowest structure with respect to M1, M2 and M3. The choice of the higher level B3LYP/6–311++G(d,p) was to ensure satisfactory results throughout analysis. A triclinic box with volume of 27 cm^3 was initially considered; a single hordenine monomer

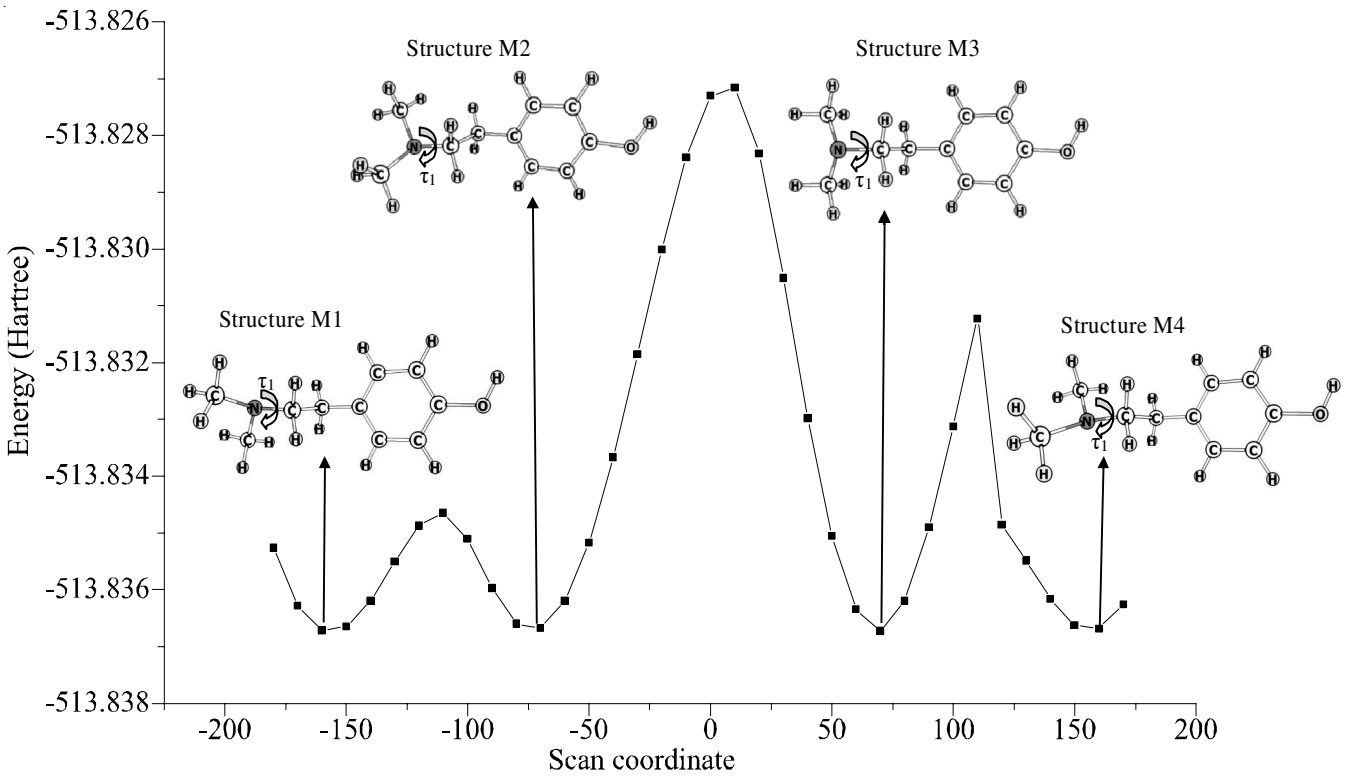

Fig. 2. PES scan curve showing the four minimum structures (M1, M2, M3 and M4) of Hordenine computed at the B3LYP/3-21G level by varying the dihedral angle τ_1

M′4 was placed at the center at a distance of 1.0 nm from the edges. After defining the box dimensions, ten M′4 monomers were added to the system with 1000 TIP4P (transferable inter–molecular potential 4P) water model as solvent and the total density of the system was 1.81 kg/L (Fig. 3). The water molecules acted as implicit solvent medium ensuring stable structure species of hordenine. Subsequent steps involved energy minimization, the first equilibration phase run at normal volume (V) and temperature (T = 295 K) for 100 ps time step, the second equilibration phase run at pressure (P = 1 bar) and temperature (T = 295 K) for 100 ps time step to achieve system stabilization and pressure convergence and finally MD production was performed for a total of 30 ns with time step of 2 fs. All the covalent bonds were constrained using the LINCS algorithm and OPLS-AA force field parameters (Table-2) as implemented in Gromacs [16]. Certain input parameters (Table-3) as required were computed from the Gaussian 09W at B3LYP/6–311++G(d, p) level of calculations [15]. During the 30 ns, the association/dissociation of the O–H···N/O–H···O bonds in the two kinds of linear dimer species were seen using visual molecular dynamics (VMD) suite (Fig. 4) [17]. To determine their relative stabilities, we ran optimization at B3LYP/6–311++G (d, p) level by varying the H···N and H···O lengths in the O–H···N/O–H···O bonds from 1.5 to 2.1 Å with an increment of 0.1 Å. We found that the O–H···N bonded dimer lies below the O–H···O bonded species by 1.255 kcal/mol. We computed the IR and Raman modes and other computational descriptors from AIM and NCI including vibrational properties from the associated VEDA and Multiwfn/VMD packages [18,19].

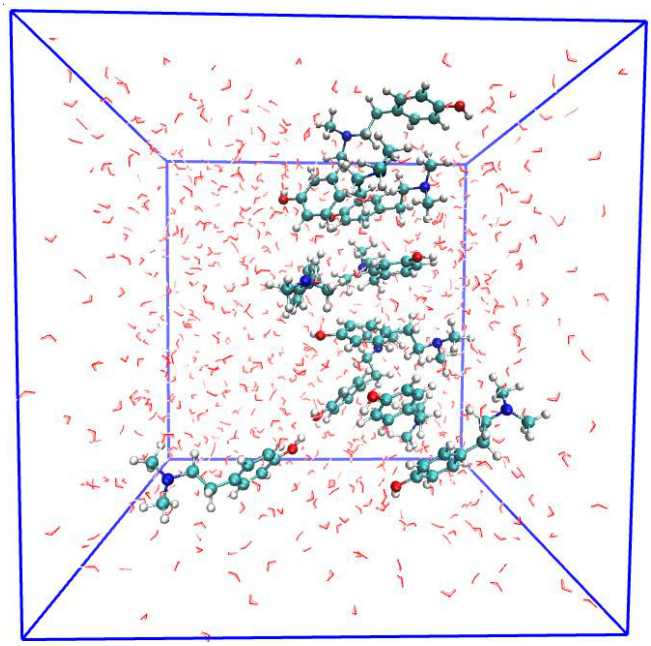

Fig. 3. Snapshots of equilibrated simulation box at 510 ps showing 10 hordenine and 1000 water molecules (TIP4P model). Hordenine molecules are shown in CPK model (water molecules are shown by red lines)

RESULTS AND DISCUSSION

Dimers structure: The intermolecular O–H···N bonded dimer (D1) and intermolecular O–H···O bonded dimer (D2), from the MD simulations in the water medium were obtained.

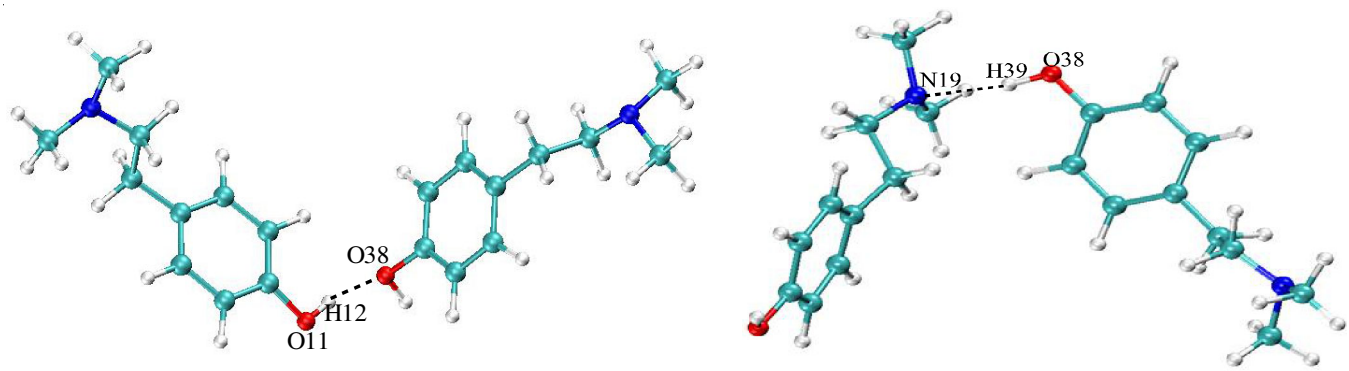

Fig. 4. Snapshots of O–H···O and O–H···N dimer structures obtained from MD simulation at different time windows

TABLE-2
LENNARD-JONES PARAMETERS OF HORDENINE STRUCTURE OBTAINED FROM OPLS-AA FORCE FIELD

Atom types[a]		σ (nm)[b]	ε (kJ/mol)[c]
Aromatic	C(OPLS_145)	0.355	0.292
	C(OPLS_147)	0.355	0.292
	C(OPLS_166)	0.355	0.292
	H(OPLS_146)	0.242	0.125
Hydroxyl	O(OPLS_167)	0.307	0.711
	H(OPLS_168)	0.000	0.000
$(CH_2)_2$	C(OPLS_149)	0.350	0.276
	C(OPLS_908)	0.350	0.276
	H(OPLS_140)	0.250	0.125
N-$(CH_3)_2$	N(OPLS_902)	0.330	0.711
	C(OPLS_905)	0.350	0.276
	H(OPLS_140)	0.250	0.125

[a]Atom types from OPLS-AA force field. [b&c]Lennord-Jones parameters.

TABLE-3
PARTIAL CHARGES OF HORDENINE OBTAINED BY B3LYP/6-311++G(d,p) LEVEL USING CHELPG CHARGES

Atom	q (a.u.)[b]	Atom	q (a.u.)[b]
C1	-0.107	H15	0.146
C2	-0.165	H16	0.133
C3	0.105	H17	0.137
C4	-0.163	H18	0.104
C5	-0.134	N19	-0.441
C6	0.252	C20	-0.251
H7	0.140	H21	0.105
H8	0.126	H22	0.142
H9	0.123	H23	0.145
H10	0.116	C24	-0.246
O11	-0.628	H25	0.142
H12	0.368	H26	0.108
C13	-0.320	H27	0.140
C14	-0.081	–	–

In order to gain insights into the structural changes of the two dimer species and characterize the O–H···N and O–H···O bonds we have computed the radial distribution functions (RDF) for them from the MD and the plots are shown in Fig. 5a-b [20]. The RDF (also known as pair distribution function) refers to an interaction between, say, an atomic species α being surrounded by a number of an atomic species, say, β, lying within a sphere of radius r around the α [21]. The size, width and positions of the peaks correspond to the structural environment surrounding the atomic species. Applying it to our context, it is the interaction between the donor (O–H)··· acceptor (N) pair in D1 and the donor (O–H)···acceptor (O) pair in D2. These interacting pairs are formed from the –O–H and N–$(CH_3)_2$ groups. In Fig. 5a-b, computed RDF values are shown on the vertical scale and the bond distances on the horizontal scale. It is apparent from Fig. 5a that the donor (O–H)···acceptor (N) pair is characterized by the first sharp but medium peak near 2.0 Å followed by a well-defined structure. The first peak value is less than the sum of the of van der Waals radii of H and N atoms, 2.75 Å and the life time of O–H···N is 35 ps. After a well-defined minimum the second peak is still smaller lying around 3 Å followed by an asymmetric broad peak up to the two tall peaks with continuum outwards. The distribution of these peaks is taken to mean a quasi-long range order within the dimer D1 species. In Fig. 5b, the very sharp first peak at 2.6 Å, refers to a relatively strong interaction between the O–H group and surrounding the O atoms. This is followed by a broader peak structure that suggests a greater number of O atoms is distributed around the O–H group, with additional peaks appearing beyond 4 Å. The first peak value of 2.6 Å is evidently less than the sum of the van der Waals radii of H and O atoms, 2.72 Å and the life time of the O–H···O is about 12 ps. Some peripheral H-bonds observed in the MD simulation between hordenine-water and water-water species having shorter life time of 6-7 ps have been ignored (Table-4).

TABLE-4
AVERAGE NUMBER OF H-BONDS PER TIME FRAME AND THEIR LIFETIMES FOR 30 ns SIMULATION DURATION

H–bonded species	Average number of H–bonds per timeframe	Lifetime of H–bonds (ps)
(O–H)···N	0.178	35.00
(O–H)···O	0.384	11.57
(O–H)···O_W	0.180	7.55
$(O–H)_W$···O_W	0.214	6.04

O_W – Oxygen in water.

To characterize the O–H···N and O–H···O bonds from the structural view-point, we have carried out analysis of the estimation of the compactness of dimer D1 structure and the structure of the two H-bonds within and between the dimer species using the RDF. The structural compactness is evaluated in terms of the radius of gyration (R_g) [22]. During the simulation process, the R_g spectrum was monitored during the formation of dimer species and any accompanying compression changes in the

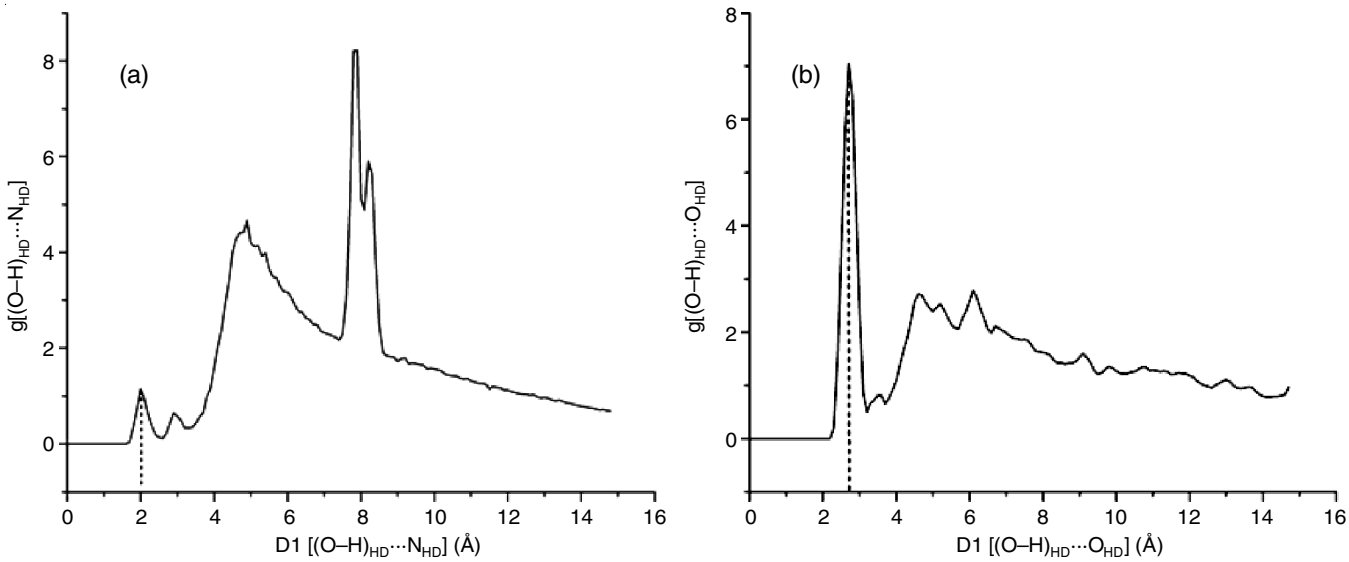

Fig. 5. RDF plots (a) the distribution of peaks refer to the O–H···N bond interaction; (b) similar distribution pattern for the O–H···O bond interaction. The RDF pattern in (a) shows relative structural order in relation to it in (b) for the dimer D1. HD refers to hordenine molecule

structures [23,24]. As illustrated in Fig. 6, the analysis of R_g shows that the O–H···O and O–H···N dimer structures exhibit compression over the simulation period. The two patterns of variations of R_g *versus* time are almost similar but R_g for the O–H···N bonded D1 dimer is shorter than for the O–H···O bonded D2 dimer (Table-5). The R_g values for both dimers ranged from 0.77 to 2.07 nm for the O–H···N dimer and 0.73 to 1.96 nm for the O–H···O dimer with the two patterns of variations of R_g *versus* time are almost similar but indicating a notable compactness during the simulation period. Further, the mean R_g value for the O–H···N dimer is 1.35 nm, being lower than that of the O–H···O dimer D2 at 1.40 nm, suggesting that the O–H···N dimer D1 exhibits more relative stability. Whereas

TABLE-5
RADII OF GYRATION (R_g), MINIMUM DISTANCES BETWEEN MONOMER SPECIES IN DIMERS AND ROOT-MEAN-SQUARE-DEVIATIONS (RMSD) OF TRAJECTORIES OF DIMERIC SPECIES AS A MEASURE OF MOBILITY FROM INITIAL TO FINAL INSTANT OF TIMES

H-bonded	Radius of gyration R_g (nm)	Minimum distance (nm)	RMSD (nm)
D1: O–H···N	1.35	1.22	1.79
D2: O–H···O	1.40	1.27	1.39

Note: By convention all the values are given in nanometers (nm).

the mean R_g for ten hordenine species was calculated to be 1.39 nm, while its value for the presence of hordenine in the water medium is slightly higher at 1.50 nm. This suggests that the

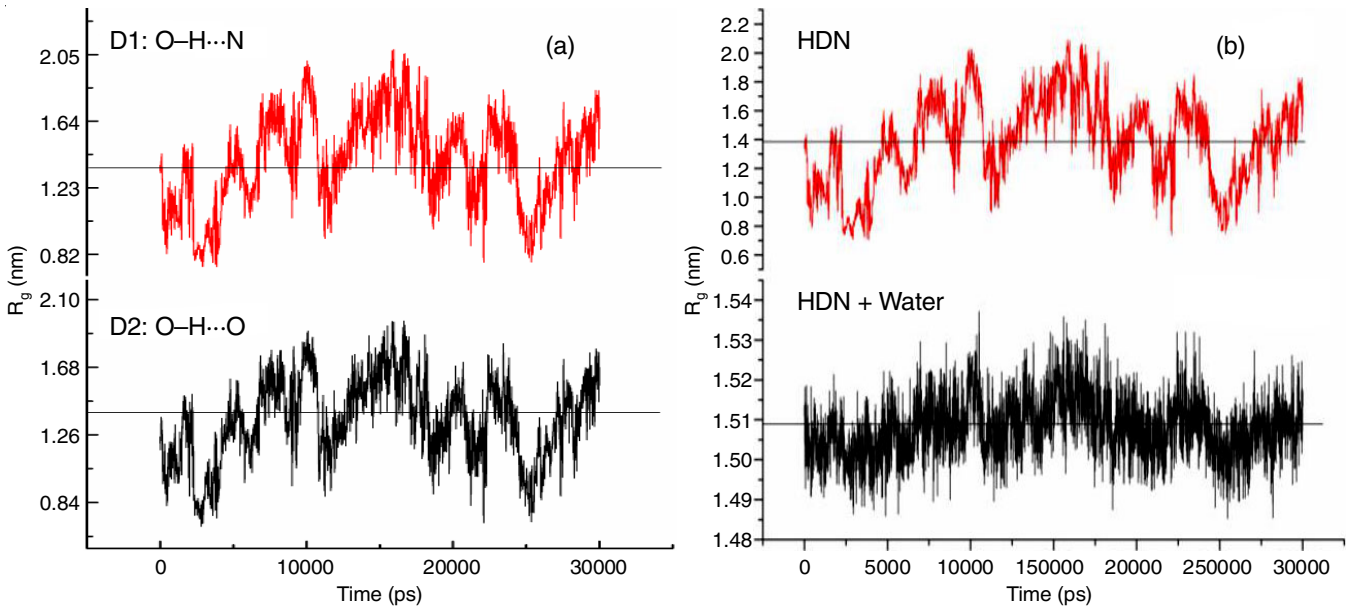

Fig. 6. The radius of gyration (R_g) of the D1(O–H···N)/D2(O–H···O) dimer structures (a) and HDN (10)* and HDN(10)* + water(1000)* systems (b) during 30 ns MD simulation process. Horizontal lines in all the four plots indicate the average R_g values. *Numbers in the brackets refer to the number of molecules

inclusion of water molecules contributes to a marginal increase in the compactness of the dimers, highlighting the influence of the solvent interaction with the hordenine species.

There is another straight forward geometrical parameter, that is 'the minimum distance' between the two monomer species in the dimer structures which we computed for comparing with R_g (Fig. 7, Table-5). It is apparent from Fig. 7 that the distances fluctuate over time with the minimum and maximum values observed are ~ 0.99 nm and 1.65 nm, respectively. The O–H···N dimer D1 shows fewer fluctuations than the O–H···O dimer D2 and the minimum distance for the O–H···N dimer D1 is slightly longer than for the O–H···O dimer D2.

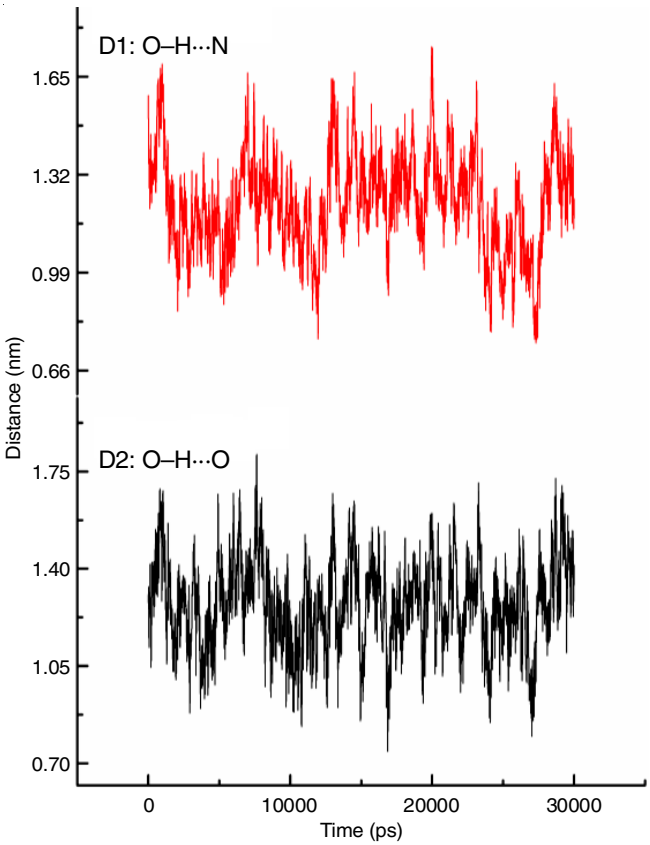

Fig. 7. Distance between the centers of two monomers in hordenine structures

RMSD values for the O–H···O and O–H···N bonded dimer D1 and D2 structures may be taken to mean the evolution of the deviations of trajectories of a given dimer, say D1 or D2, or more specifically the distances of the atoms at time, say 't = τ' (where τ refers to the duration), in relation to the distances at t = 0 (Fig. 8). In computing RMSD, the trajectories of a reference structure, say D1, as function of time is compared to its reference structure to understand mobility during the MD simulation run. Higher RMSD value for the O–H···N dimer may suggest more mobility than for the O–H···O bond [25].

The O–H···N bonded dimer D1 with atom numbering scheme is shown in Fig. 9. The computed structural H-bonded parameters like bond lengths and bond angles are presented in Table-6. These values are conceptually compared with the reported XRD data, as the computed and experimental structures do not strictly align, except for a general agreement [10,26].

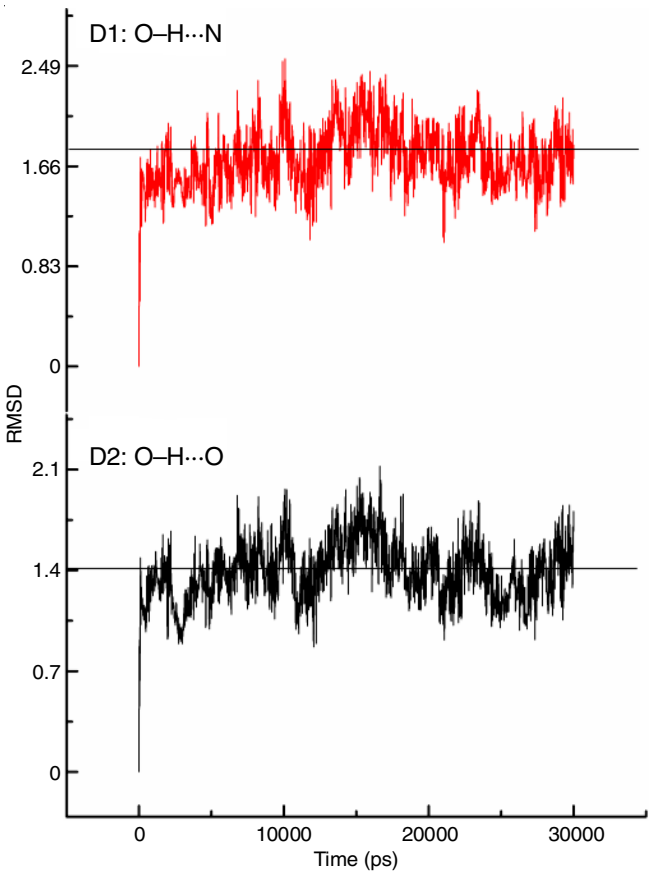

Fig. 8. In RMSD calculation one structure from a trajectory is compared to a reference structure to understand mobility of the O–H···O and O–H···N bondedbonds during MD simulation

TABLE-6
COMPUTED H-BOND PARAMETERS IN THE O–H···N BONDED DIMER D1OF HORDENINE, CALCULATED AT B3LYP/6-311++G (d,p) LEVEL

H–bond parameters D(X–H···Y) (Å)		
d(H39···N19)	1.847	–
D(O38···N19)	2.813	2.750
H–bonding angle (∠X–H···Y) (°)		
O38-H39···N19	163.8	–

It is observed that d = 1.847 Å being shorter than the sum of van der Waals radii of H and N, 2.750 Å and bond angle X–Ĥ ···A= 175.4º, both values suggest that the O38–H39···N19 bond is a stronger one. The geometry of D1 has shown attendant changes due to dimerization which includes stretching, bending and torsional strains of the bonds in the two rings and bonds in the –O–H and N–$(CH_3)_2$ moieties. It has been pointed out the role of the intra-molecular C–H···N hyperconjugative interaction in the monomer species of hordenine to be discussed later. It was observed that the H23 in one of the CH_3 groups bonds with N19 giving rise to C20–H23···N19 bond and likewise the C24–H27···N19 bond from another methyl group. All of these H–bonds may provide more stability for D1 structure. All the computed geometrical parameters are given in Table-7.

Vibrational structure: The dimer D1 structure is bound by the intermolecular O–H···N bond with O38, H39, N19 atoms involved and N19 atom is bonded to C14, C20 and C24 atoms.

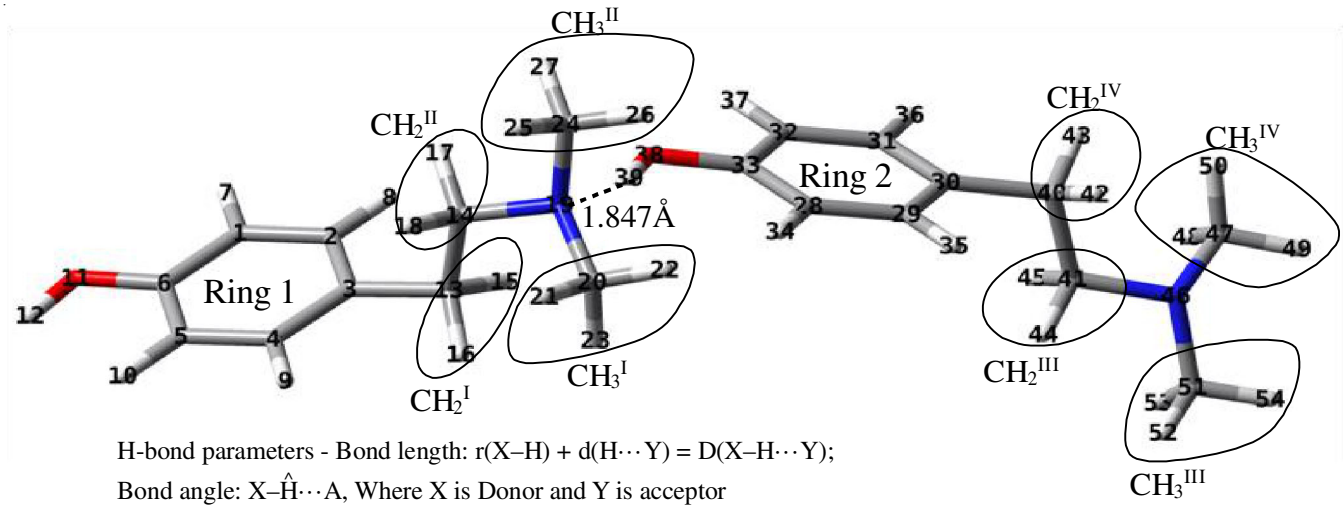

Fig. 9. Optimized O–H···N bonded dimer D1 computed at B3LYP/6-311++G(d, p). The d = 1.847 Å value is for the bond distance H39···N19. For clarity, the ethyl and dimethyl moieties are labeled and shown encircled

TABLE-7a
COMPUTED BOND LENGTHS IN THE O–H···N BONDED DIMER D1OF HORDENINE WHICH ARE NOTIONALLY COMPARED WITH XRD VALUES. DEVIATIONS SHOWN ARE SUGGESTIVE OF THE PERFORMANCE OF B3LYP/6-311++G (d,p) LEVEL

Parameters	Bond length (Å)		Deviation	Parameters	Bond length (Å)
	D1	XRD*	δ		D1
C1–C2	1.390	1.380	0.010	C28–C29	1.394
C1–C6	1.395	1.378	0.017	C28–C33	1.399
C2–C3	1.401	1.377	0.024	C29–C30	1.397
C3–C4	1.396	1.374	0.022	C30–C31	1.400
C4–C5	1.394	1.380	0.014	C31–C32	1.390
C5–C6	1.394	1.369	0.025	C32–C33	1.398
C1–H7	1.083	0.970	0.113	C28–H34	1.084
C2–H8	1.085	0.940	0.145	C29–H35	1.086
C4–H9	1.085	0.936	0.149	C31–H36	1.086
C3–C13	1.513	1.508	0.005	C30–C40	1.512
C5–H10	1.086	0.924	0.162	C32–H37	1.083
C6–O11	1.370	1.360	0.010	C33–O38	1.358
O11–H12	0.962	0.905	0.057	O38–H39	0.990
C13–C14	1.538	1.508	0.030	C40–C41	1.539
C13–H15	1.093	1.003	0.090	C40–H42	1.094
C13–H16	1.093	0.968	0.125	C40–H43	1.093
C14–H17	1.093	0.996	0.097	C41–H44	1.094
C14–H18	1.104	0.927	0.177	C41–H45	1.107
C14–N19	1.476	1.475	0.001	C41–N46	1.463
N19–C20	1.465	1.457	0.008	N46–C47	1.457
N19–C24	1.467	1.458	0.009	N46–C51	1.457
C20–H21	1.102	1.003	0.099	C47–H48	1.107
C20–H22	1.092	0.977	0.115	C47–H49	1.092
C20–H23	1.090	0.919	0.171	C47–H50	1.090
C24–H25	1.102	1.031	0.071	C51–H52	1.092
C24–H26	1.092	0.994	0.098	C51–H53	1.106
C24–H27	1.091	0.929	0.162	C51–H54	1.093
H–bond parameters D(X–H···Y)					
d(H39···N19)	1.847	—			
D(O38···N19)	2.813	2.750			

Note: *XRD reference [Ref. 10]

The results related to the structure of dimer D1, the molecular model in the investigation, are of interest here. The IR spectral evidence for the presence of O–H···N bond is readily correlated to the frequency at 3108 cm^{-1} due to the stretching mode of the O38–H39 bond since the computed frequency is at 3154 cm^{-1} (Fig. 10). There is another computed frequency at 3709 cm^{-1} which is correlated to a weak band observed at 3697 cm^{-1} and is assigned to the characteristic stretching mode of the free O38–H39 bond. It follows that the stretching mode of the O38–H39 bond in the intermolecular O–H···N bond is down-

TABLE-7b
COMPUTED BOND ANGLES OF THE BONDS IN THE O–H···N DIMER D1STRUCTURE OF HORDENINE WHICH ARE NOTIONALLY COMPARED WITH XRD VALUES. DEVIATIONS SHOWN ARE SUGGESTIVE OF THE PERFORMANCE OF B3LYP/6-311++G (d,p) LEVEL

Parameters	Bond angle (º)		Deviation	Parameters	Bond length (Å)
	D1	XRD	δ		D1
C1–C2–C3	121.6	122.1	0.409	C28–C29–C30	121.7
C1–C2–H8	119.1	121.3	1.813	C28–C29–H35	118.9
C2–C1–C6	119.7	120.5	0.639	C29–C28–C33	120.2
C2–C1–H7	121.2	121.0	0.165	C29–C28–H34	120.0
C6–C1–H7	119.1	118.4	0.591	C33–C28–H34	119.8
C2–C3–C4	117.8	116.7	0.942	C29–C30–C31	117.4
C3–C2–H8	119.3	116.3	2.579	C30–C29–H35	119.4
C3–C4–C5	121.4	121.8	0.328	C30–C31–C32	121.7
C3–C4–H9	119.7	121.9	1.804	C30–C31–H36	119.4
C5–C4–H9	118.9	116.3	2.235	C32–C31–H36	118.9
C4–C5–C6	119.8	120.5	0.580	C31–C32–C33	120.2
C1–C6–C5	119.8	118.3	1.267	C28–C33–C32	118.9
C4–C3–C13	121.4	122.8	1.140	C31–C30–C40	121.3
C2–C3–C13	120.8	120.5	0.248	C29–C30–C40	121.3
C4–C5–H10	120.1	120.5	0.331	C31–C32–H37	121.0
C6–C5–H10	120.1	117.9	1.865	C33–C32–H37	118.7
C1–C6–O11	117.5	123.5	4.858	C28–C33–O38	123.2
C5–C6–O11	122.8	118.2	3.891	C32–C33–O38	117.9
C6–O11–H12	109.7	114.4	4.108	C33–O38–H39	112.6
C3–C13–C14	111.6	111.1	0.450	C30–C40–C41	112.3
C3–C13–H15	109.9	109.9	0.000	C30–C40–H42	110.3
C3–C13–H16	109.2	107.4	1.675	C30–C40–H43	109.1
C14–C13–H15	108.6	108.5	0.092	C41–C40–H42	108.1
C14–C13–H16	110.3	109.4	0.822	C41–C40–H43	110.0
H15–C13–H16	107.3	110.4	2.807	H42–C40–H43	106.8
C13–C14–H17	108.5	110.8	2.075	C40–C41–H44	108.1
C13–C14–H18	109.6	112.5	2.577	C40–C41–H45	109.3
C13–C14–N19	114.1	114.2	0.087	C40–C41–N46	113.7
H17–C14–H18	106.9	107.6	0.650	H44–C41–H45	106.4
H17–C14–N19	107.1	110.0	2.636	H44–C41–N46	107.5
H18–C14–N19	110.4	107.6	2.602	H45–C41–N46	111.3
C14–N19–C20	112.5	111.3	1.078	C41–N46–C47	113.0
C14–N19–C24	110.2	109.1	1.008	C41–N46–C51	111.3
C20–N19–C24	110.4	109.6	0.729	C47–N46–C51	110.8
N19–C20–H21	112.0	109.9	1.910	N46–C47–H48	112.6
N19–C20–H22	109.5	109.2	0.274	N46–C47–H49	109.5
N19–C20–H23	110.6	108.5	1.935	N46–C47–H50	110.7
H21–C20–H22	108.1	113.5	4.757	H48–C47–H49	108.0
H21–C20–H23	108.6	101.2	7.312	H48–C47–H50	108.2
H22–C20–H23	107.9	110.0	1.909	H49–C47–H50	107.6
N19–C24–H25	112.2	111.4	0.718	N46–C51–H52	109.9
N19–C24–H26	109.7	112.3	2.315	N46–C51–H53	113.0
N19–C24–H27	109.7	104.9	4.575	N46–C51–H54	109.7
H25–C24–H26	108.4	110.7	2.077	H52–C51–H53	108.1
H25–C24–H27	108.6	103.6	4.826	H52–C51–H54	108.1
H26–C24–H27	108.2	113.2	4.416	H53–C51–H54	107.9
H–bonding angle (X–? ···A)					
O38–H39···N19	163.8°	175.4°	6.613		

Note: *XRD reference [Ref. 10]

shifted to absorb at 3108 cm^{-1} from its free OH–bond value at 3697 cm^{-1}as in phenol [27-29]. The IR spectral region from 3110 to 2520 cm^{-1} evidently shows broad band features with FWHM ~ 600 cm^{-1} being the signature of H-bonding in D1. However, it is to be noted that the IR spectral features such as the broad band width and intensity associated with the intermolecular O–H···N bond when compared with that of a typical broad band features due to the O–H···O bond are less striking on account of relatively less anharmonicity of the O–H modes of the O–H···N bond. A large number of sharp and intense observed IR and Raman bands seem to suggest a dimer molecular model is the basis of their origin. All things considered we assume that the dimer D1 structure bound by the intermolecular O–H···N bond is the model for understanding the

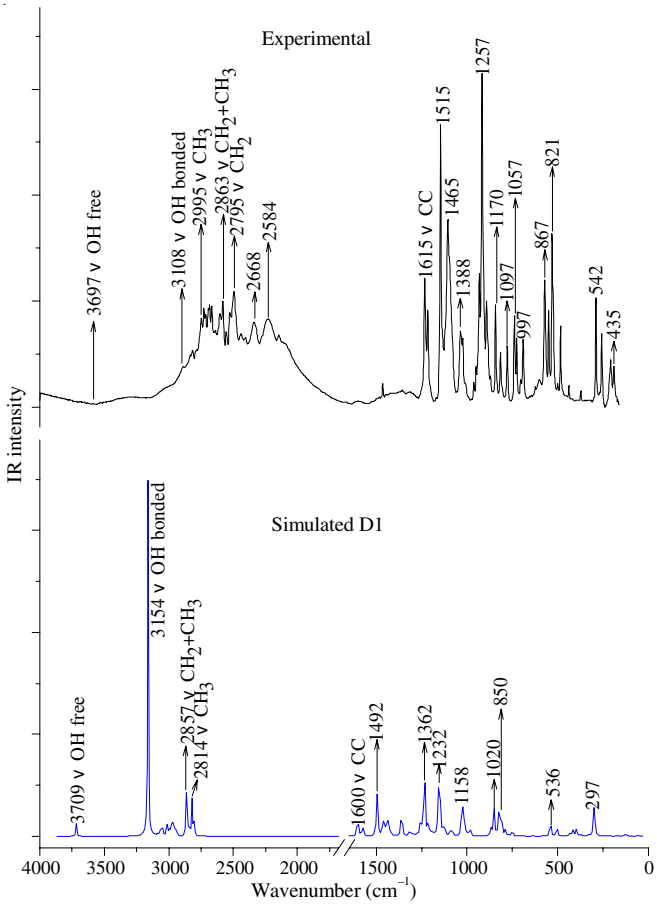

Fig. 10. Experimental IR spectrum with the simulated spectrum for D1 of hordenine. For fair comparison, the intensities of the bands in the simulated spectrum (which are otherwise weak) in the region 1500–400 cm^{-1} are suitably scaled [ν-refers to stretching frequency]

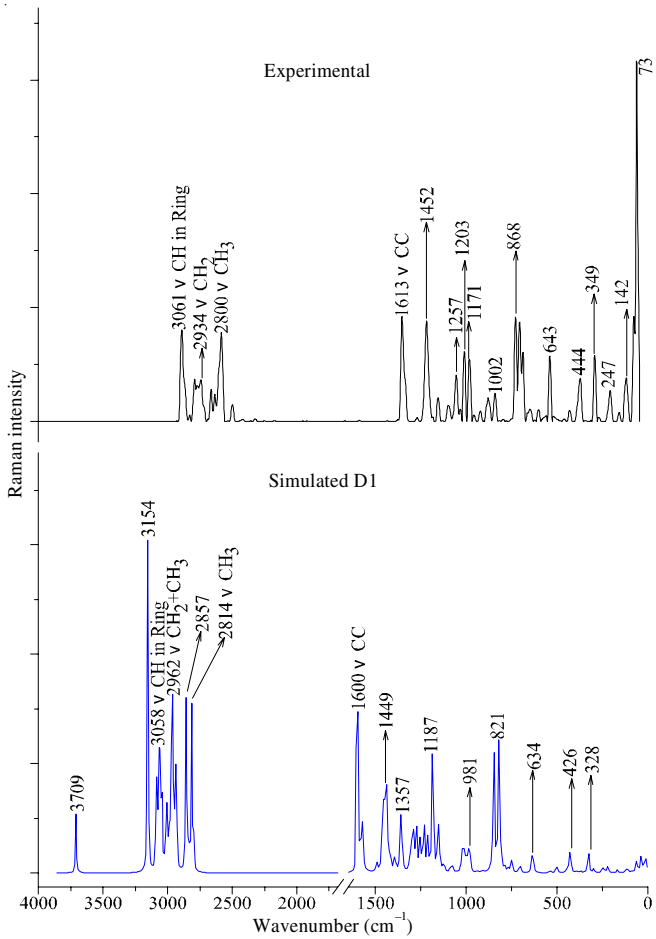

Fig. 11. Experimental Raman spectrum with the simulated spectrum for D1 of hordenine. For fair comparison, the intensities of the bands in the simulated spectrum (which are otherwise weak) in the region 1500–400 cm^{-1} are suitably scaled [ν-refers to stretching frequency]

experimental IR and Raman vibrational structures. It is therefore expected that the computed vibrational structure of D1 agree with the IR and Raman mode structures and all the vibrational spectra are shown in Figs. 10 and 11. The bands associated with the CH, CH and CH_3 moieties have maintained their characteristic features both with respect to band positions and intensities. The asymmetric stretching vibration of the CH moiety generally occurs between 2950 and 2955 cm^{-1}. In the present case, it is observed as IR band at 2981 cm^{-1} and Raman band at 2976 cm^{-1} and the computed value is 2979 cm^{-1}. The symmetric stretching modes of the CH_2 moiety are observed as IR bands at 2881 and 2863 cm^{-1} and as Raman bands at 2868 and 2844 cm^{-1}. The corresponding computed values are 2818 cm^{-1} and 2813 cm^{-1}. The dimethyl moiety is bonded to the NH_2 group, so the aliphatic N–$(CH_3)_2$ exhibits asymmetric stretching modes within the 2825–2810 cm^{-1} and 2775–2765 cm^{-1} regions. The asymmetric stretching mode of the CH_3 moiety is observed as IR band at 2995 cm^{-1} and as Raman band at 3007 cm^{-1}. The corresponding computed values are 2993 and 2991 cm^{-1}. The modes of the C–H bonds in the phenyl ring, CH_2 and CH_3 moieties are characteristically Raman sharp bands. The torsional mode associated with the OH-OH bond identified as IR band at 642 cm^{-1} with a strong Raman band at 643 cm^{-1} and computed at 635 cm^{-1}. The Raman and computed bands with frequencies below 200 cm^{-1} are identified as the torsional vibrational modes since they are genuinely less vibrational and more torsional and at best they characterize the deformation of the dimer D1 structure as a whole. It is on account of the multiple deformations of the structure of D1 that gives rise to strong Raman bands in the region 200-50 cm^{-1} [30]. For the sake of brevity, we have presented selected IR, Raman and computed modes with assignments in Table-8 [31,32].

Electronic structure

Natural bond orbital analysis: After structural and vibrational characterization of the O–H···N bond in D1, it is of interest to study its electronic structure from the perspective of the molecular orbital picture. The natural bond orbital (NBO) approach deals with the different molecular orbitals and their overlap for representing the donor-acceptor interaction in H-bonding [34]. We computed stabilization energy ($E^{(2)}$), natural populations and orbital occupancies by carrying out NBO analysis [35]. The stabilization energy ($E^{(2)}$) is ~17 kcal/mol (~0.73 eV) for the orbital overlap between lone–pair orbital n_1(N19) and anti–bonding orbital σ*(O38–H39) (Fig. 12 and Table-9). There is the C–H···N bond involved as the intramolecular hyperconjugative interaction in the phenyl ring R1 as n_1(N19)

TABLE-8
SELECTED ASSIGNMENTS OF EXPERIMENTAL AND COMPUTED VIBRATIONAL WAVENUMBERS (cm^{-1}) OF HORDENINE DIMER D1

Wavenumbers			δ_{D1}	Intensity[b] D1		Assignments[c] [%PED]
IR	Raman	D1[a]		I_{IR}	I_{Ra}	
3697 vw	–	3709	0.3	72.7	149.5	OH free stretching
3108 vw	–	3154	1.4	1878.2	658.5	O–H···N bonded stretching on D1
2668 m	–	–	–	–	–	1388 + 1274 [HCH wagging on CH_3^{III} + HCN wagging on CH_2^{I}]
2582 ms	–	–	–	–	–	1302 + 1274 [CC sym. stretching CH_2^{III} + HCN wagging on CH_2^{I}]
2518 w	–	–	–	–	–	1615 + 903 [CC sym. stretching on R1 + HCCO torsion on R2]
1874 s	–	–	–	–	–	952 + 925 [HCCC torsion on R1 + HCCC torsion on R1]
1747 w	–	–	–	–	–	952 + 789 [HCCC torsion on R1 + HCCC torsion on R2]
1379 s	1376 m	1362	1.2	18	13.3	HCNC torsion + HCN twisting on R2
1257 vs	1257 s	1256	0.0	49.3	11.1	HCNC torsion on R2 + NC sym. stretching on N–(CH_2^{IV})
1229 m	–	1234	0.4	63.2	11.8	OC sym. stretching on R2
–	1203 s	1214	0.9	15.5	10.1	HCC bending on CH_2^{III} + CH_2^{IV}
1170 s	1171 s	1158	1.0	17.2	3.1	HOH bending + CC sym. stretching R1 + HOHO bonded torsion
1057 s	1047 m	1029	2.6	34.1	2.2	NC + NC sym. stretching on N–$(CH_2)_2$ + CC sym. stretching on $(CH_2)_2$ + HCNC torsion on N–$(CH_2)_3$
1044 s	–	1020	2.2	17.8	0.6	NC + NC sym. stretching on N–$(CH_2)_2$ + CC sym. stretching on $(CH_2)_2$ + HCNC torsion on N–$(CH_2)_3$
867 s	868 s	867	0.0	23.0	1.0	NC sym. stretching N–$(CH_2)_2$ on R1 + NC
844 s	842 s	850	0.7	19.6	32.0	NC + NC sym. stretching N–$(CH_2)_2$ on R2
821 s	820 m	824	0.3	14.8	21.2	CC + CCC bending + OC ring stretching on R2
642 m	643 s	634	0.7	0.8	5.8	CCC + CCC + CCC ring bending on R2
542 s	547 vw	536	1.1	24.6	0.5	OCCC + CCCC + CCC out of plane bending on R2
435 s	444 s	436	0.2	0.5	1.6	CNC bending on N–$(CH_3)_2$ on R2
–	247 m	244	1.2	0.2	0.3	HCNC + HCNC + HCNC torsion on $(CH_2)_2$–N–$(CH_3)_2$ on R1
–	73 vs	88	20.5	0.5	0.5	CCOH torsion + CCCC out of plane bending + CCC bending + HOC bending on R1

Note: [a]Selected frequencies are considered in both experimental and theoretical spectra. Frequencies are scaled by 0.9688 [Ref. 33].
% δ_{D1} = deviation is defined as: [{(computed freq–exptl freq)}/exptl freq] × 100.
R1 and R2 refer to ring1 and ring2; CH_3^{I}, CH_3^{II}, CH_2^{I} and CH_2^{II} are from ring1 and CH_3^{III}, CH_3^{IV}, CH_2^{III} and CH_2^{IV} are from ring2.
[b]Refers to computed IR intensity (I_{IR}) in km/mole, Raman intensity (I_{Ra}) in $(Å)^4$/amu. [c]PED contribution in %.
Intensities of experimental bands are described as: vs = very strong. s = strong. m = medium. w = weak. vw = very weak.

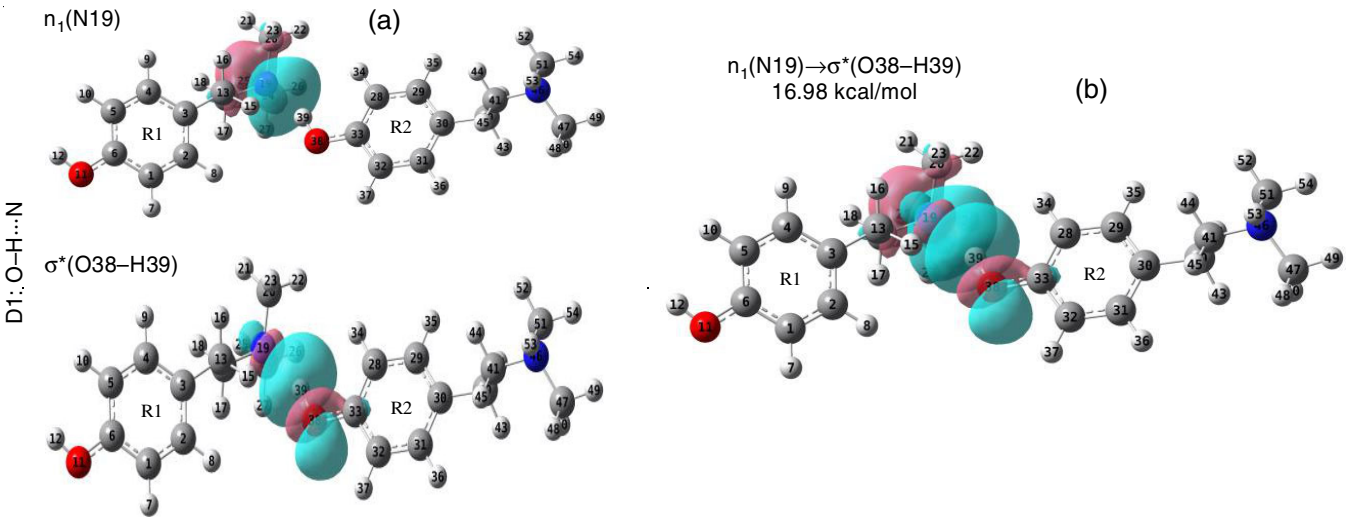

Fig. 12. (a) Lone–pair orbital n_1(N19) and anti-onding orbital σ*(O38–H39); (b) the overlap of the lone-pair orbital n_1(N19) and anti-bonding orbital σ*(O38-H39) representing O–H···N bond in the dimer D1 structure of hordenine

→σ*(C14–H18) and in the phenyl ring R2 at n_1(N46)→σ*(C41–H45); similarly, the interactions between N and $(CH_3)_2$ groups is given as n_1(N19)→σ*(C20–H21) and n_1(N19)→σ*(C24–H25) in the ring R1 with stabilization energies at 6.83 and 6.49 kcal/mol. Natural populations of the charges provide charge transfers or conjugate interactions across the orbital overlaps as demonstrated by the magnitudes shown in Table-10. According to the NBO procedure, the strength of O–H···N bond is determined by assessing the difference in occupancies between bonding and anti–bonding natural bond orbitals [36]. Table-11 shows the occupancies, NBO descriptions and polarization coefficients of 's' characters (in %) for each atom in the D1 structure. As observed in Table-11, the s character of O38–H39 hybrid orbitals contributes significantly to the strength

TABLE-9
STABILIZATION ENERGY $E^{(2)}$ FOR THE –O–H···N BONDING AND HYPERCONJUGATIVE INTERACTION OF C–H···N BONDING IN D1 STRUCTURE

D1		Donor (i)	Acceptor (j)	$E^{(2)}$ (kcal/mol)*
O–H···N		n_1(N19)	σ*(O38–H39)	16.98
C–H···N	Ring 1	n_1(N19)	σ*(C14–H18)	6.95
		n_1(N19)	σ*(C20–H21)	6.83
		n_1(N19)	σ*(C24–H25)	6.49
	Ring 2	n_1(N46)	σ*(C41–H45)	9.18
		n_1(N46)	σ*(C47–H48)	8.78
		n_1(N46)	σ*(C51–H53)	8.74

$$*-E^{(2)} = -n\frac{F_{ij}^2}{\varepsilon_j - \varepsilon_i}$$

of the O–H···N bond. This influence is evident in the geometry of D1 in which the O38–H39 bond shows elongation by 0.085 Å compared to its value in the XRD monomer structure [37]. The elongation gives rise to a red shift of ~16 % in the stretching frequency of O11–H12 bond from its computed monomeric value. Further, it is observed that the O–H···N and C–H···N bonds show electronic polarizations that can be represented in terms of molecular orbitals. The σ(O38–H39) is strongly polarized towards the H39 atom and σ*(O38–H39) is strongly polarized towards the O38 atom. In addition, the hyperconjugative interactions of σ(C14–H18), σ(C20–H21), σ(C24–H25), σ(C41–H45), σ(C47–H48) and σ(C51–H53) are characterized by strong polarization towards the H atoms, while σ*(C14–H18), σ*(C20–H21), σ*(C24–H25), σ*(C41–H45), σ*(C47–H48) and σ*(C51–H53) display strong polarization towards

TABLE-10
NATURAL ATOMIC CHARGES CALCULATED BY B3LYP/6-311++G(d,p) FOR D1 STRUCTURE

Atom No.	Charge in a.u	Atom No.	Charge in a.u	Atom No.	Charge in a.u
C1	-0.24283	N19	-0.59267	H37	0.21071
C2	-0.17777	C20	-0.35740	O38	-0.72182
C3	-0.06051	H21	0.17283	H39	0.49322
C4	-0.18158	H22	0.19495	C40	-0.39826
C5	-0.27762	H23	0.19838	C41	-0.15275
C6	0.31051	C24	-0.35413	H42	0.20840
H7	0.21783	H25	0.17228	H43	0.19735
H8	0.20953	H26	0.19651	H44	0.19026
H9	0.20044	H27	0.20192	H45	0.15994
H10	0.19939	C28	-0.27999	N46	-0.56033
O11	-0.67494	C29	-0.18333	C47	-0.35717
H12	0.46571	C30	-0.06883	H48	0.15865
C13	-0.40837	C31	-0.18212	H49	0.19126
C14	-0.15395	C32	-0.24750	H50	0.19065
H15	0.22274	C33	0.31817	C51	-0.35091
H16	0.19867	H34	0.19739	H52	0.19030
H17	0.20092	H35	0.19789	H53	0.15899
H18	0.17096	H36	0.19840	H54	0.18962

TABLE-11
NBO OCCUPANCY, POLARIZATION COEFFICIENTS, ORBITAL DESCRIPTIONS AND 's' CHARACTER FOR DIMER D1 STRUCTURE OF HORDENINE

NBOs	Occupancy	Polarization coefficients (%)		Description of NBO	Contribution of 's' character (%)	
Ω/Ω* (X–H)	q	c_X^2	c_H^2	$\Omega = c_X h_X + c_H h_H$; $\Omega^* = c_X h_X - c_H h_H$	X	H
σ(O38–H39)	1.98744	77.11	22.89	$0.8781(sp^{2.84})$O38 + 0.4785(*sp*)H39	26.02	99.77
σ*(O38–H39)	0.05687	22.89	77.11	$0.4785(sp^{2.84})$O38 – 0.8781(*sp*)H39		
σ(C14–H18)	1.98499	59.25	40.75	$0.7698(sp^{3.21})$C14 + 0.6383(*sp*)H18	23.75	99.96
σ*(C14–H18)	0.03043	40.75	59.25	$0.6383(sp^{3.24})$C14 – 0.7698(*sp*)H18		
σ(C20–H21)	1.99454	59.31	40.69	$0.7701(sp^{2.95})$C20 + 0.6379(*sp*)H21	25.33	99.96
σ*(C20–H21)	0.02302	40.69	59.31	$0.6379(sp^{2.96})$C20 – 0.7701(*sp*)H21		
σ(C24–H25)	1.99511	59.28	40.72	$0.7699(sp^{2.93})$C24 + 0.6381(*sp*)H25	25.45	99.96
σ*(C24–H25)	0.02265	40.72	59.28	$0.6381(sp^{2.98})$C24 – 0.7699(*sp*)H25		
σ(C41–H45)	1.98470	58.92	41.08	$0.7676(sp^{3.23})$C41 + 0.6410(sp)H45	23.54	99.96
σ*(C41–H45)	0.03763	41.08	58.92	$0.6410(sp^{3.24})$C41 – 0.7676(*sp*)H45		
σ(C47–H48)	1.99492	58.85	41.10	$0.7671(sp^{2.97})$C47 + 0.6415(*sp*)H48	25.12	99.96
σ*(C47–H48)	0.03014	41.10	58.85	$0.6415(sp^{2.98})$C47 – 0.7671(*sp*)H48		
σ(C51–H53)	1.99531	58.87	41.13	$0.7673(sp^{2.96})$C51 + 0.6413(*sp*)H53	25.23	99.96
σ*(C51–H53)	0.03006	41.13	58.87	$0.6413(sp^{2.96})$C51 – 0.7673(*sp*)H53		
n_1(N19)	1.85854			$sp^{5.38}$	15.67	
n_1(N46)	1.87672			$sp^{5.89}$	14.51	

Note: Ω/Ω*: Bonding/Anti–bonding orbitals on donor (X) and hydrogen (H) atoms respectively.
c_X, c_H = Polarization coefficients; h_X,h_H = NHO atom type X and H respectively.

the C atoms. The lone–electron pair orbital n_1(N19) and n_1(N46) show $sp^{5.38}$, $sp^{5.89}$ character, respectively.

Molecular electrostatic potential analysis: After the NBO representation of the O–H···N and C–H···N bonds, it is appropriate to proceed to represent the two H-bonds in terms of a 3D molecular electrostatic potential (MEP) surface centered about the dimer D1 (Fig. 13). Conventionally a colour code is used for visualizing the regions: the most negative potential corresponds to the red region and the most positive potential corresponds to the blue region; whereas the intermediate colours linearly correspond to all the possible values. In this context, the MEP provides charge build-up all over the dimer D1 structure with the O–H···N bonding.

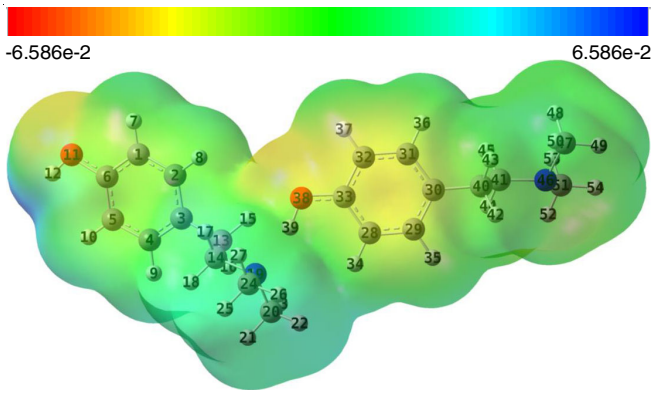

Fig. 13. Molecular electrostatic potential surface (MEP) for dimer D1 of hordenine. The colour code spectra of the potential values are shown in the range of -6.586e-2 to +6.586e-2: the red colour and blue colour correspond to the most negative potential and the most positive potential respectively. The O–H···N bonding lies in the orange-yellow region corresponding to some degree of negative potential

AIM and NCI analysis: Previously, the roles of NBO and MEP in characterizing O–H···N and C–H···N bonds were discussed. Another way of looking at these polarized H-bonds is to apply Bader's quantum theory of atoms-in-molecules (QTAIM). QTAIM uses the electron density as the best descriptor for characterizing the H-bonds by defining the molecule as the region of electrons and nuclei that lie within zero-flux surfaces surrounding the nuclei [38]. The interatomic forces associated with the nuclei and electrons within the molecule manifest by way of different forms of electronic charge distributions. The electronic charge distribution is technically called 'electron density, $\rho(r_{electronic}, R_{nuclear}) = \rho(r, R)$ or more commonly $\rho(r)$ [39]. The $\rho(r)$, being an observable, is a scalar field in 3D space with topological features which define an atom in the molecule. Thus a topological space exists where the first derivative of $\rho(r)$ (*i.e.* $\nabla\rho(r)$) vanishes at 'critical points (CP)' corresponding to the value of $\rho(r_c)$ being a minimum, maximum and a saddle point. A CP is given in terms of its rank and signature. By rank we mean the number of non–zero eigen values corresponding to non–zero curvatures of $\rho(r_c)$ at a CP and signature is the algebraic sum of the signs of eigen values. The extremum of the CP is determined by calculating the sign of the second order derivatives, $\nabla^2\rho(r_c)$ (also referred to as Laplacian). The values of $\nabla^2\rho(r_c)$ are the elements of the Hessian matrix for $\rho(r_c)$ and its appropriate diagonalization give the desired eigen values mentioned above. In present analysis, the bond critical points (BCP) approach is used. The BCP refers to a point on that axis where $\rho(r)$ is a minimum, the axis being perpendicular to the plane defined by the two negative curvatures. In that plane $\rho(r)$ is a maximum at the positions of nuclei of atoms in the molecule. Technically, this situation is described as (3, –1): the two curvatures are negative and $\rho(r_c)$, being a maximum at r_c, is the minimum at CP in the plane determined by the axes of curvatures. There is a third axis being perpendicular to this plane where $\rho(r_c)$ is a maximum at CP. In the context of characterizing chemical bonds, the extrema of CP are BCPs [40,41].

The molecular graph in Fig. 14a-b shows the interaction between H39 and N19 atoms with BCP index 104 and 2D plot of the $\rho(r_c)$ and $\nabla^2\rho(r_c)$ for the O38–H39···N19 bond. Table-12 presents the values for $\rho(r_c)$ and $\nabla^2\rho(r_c)$ at the BCP, essential interaction energy (E_{HB}) and other topological parameters. For the H39···N19 bond, $\rho(r_c)$ is 0.040 a.u. and $\nabla^2\rho(r_c)$ is +0.092 a.u. indicating a charge depletion around the H39 atom. Similar non–covalent interactions are observed in the O38···H15, H22–H34 and H43–H50 bonds for which $\nabla^2\rho(r_c)$ values are positive. The remaining all other bonds have negative $\nabla^2\rho(r_c)$ values, suggesting a purely covalent character (Table-13) [42]. Further, it should be pointed out that the C–H bonds show much higher negative values of $\nabla^2\rho(r_c)$ because of the native aromatic ring character. Local charge concentration (dotted lines) and local charge depletion (solid lines) with bond paths (BP) being indicated by BCP are shown in Contour Plot (Fig. 14b). The dotted lines characterize the interatomic regions and are concentrated around the O39 and N19 atoms in the contour map. The solid line indicates the depletion of charge around the H39···N19 bond as seen in the molecular graph (Fig. 14a). Futhermore, another important parameter is potential energy density $V(r_c)$ correlated to the H–bond energy. The interaction energy at BCP index (104) was calculated as $E_{HB} = (1/2)\, V(r_c) = -9.734$ kcal/mol which falls in the category of strong H–bond. Following Rozas *et al.* [43], $\nabla^2\rho(r_c) = 0.092$ au >0 and H(r) = –0.004 au < 0 indicating that the O38–H39···N19 bond is a stronger H–bond. Thus, all these results are consistent with the H–bond characterizations [43].

TABLE-12
TOPOLOGICAL PARAMETERS COMPUTED AT THE 'BOND CRITICAL POINT' (BCP) FOR THE O–H···N BOUND D1 STRUCTURE OF HORDENINE. (ALL PARAMETER UNITS ARE IN a.u. EXCEPT FOR INTERACTION ENERGY, E_{HB})

Parameters	O38–H39···N19(104*)
$\rho(r_c)$	0.040
$V(r_c)$	–0.031
$\nabla^2\rho(r_c)$	0.092
G(r)	0.027
H(r)	–0.004
E_{HB} (kcal/mol)	–9.734

*Refers to BCP for the H···N bond path.

Since H–bonds belong to the class of non–covalent interactions (NCI), it is of interest to compare and contrast with two other common non-covalent interactions, namely, the van

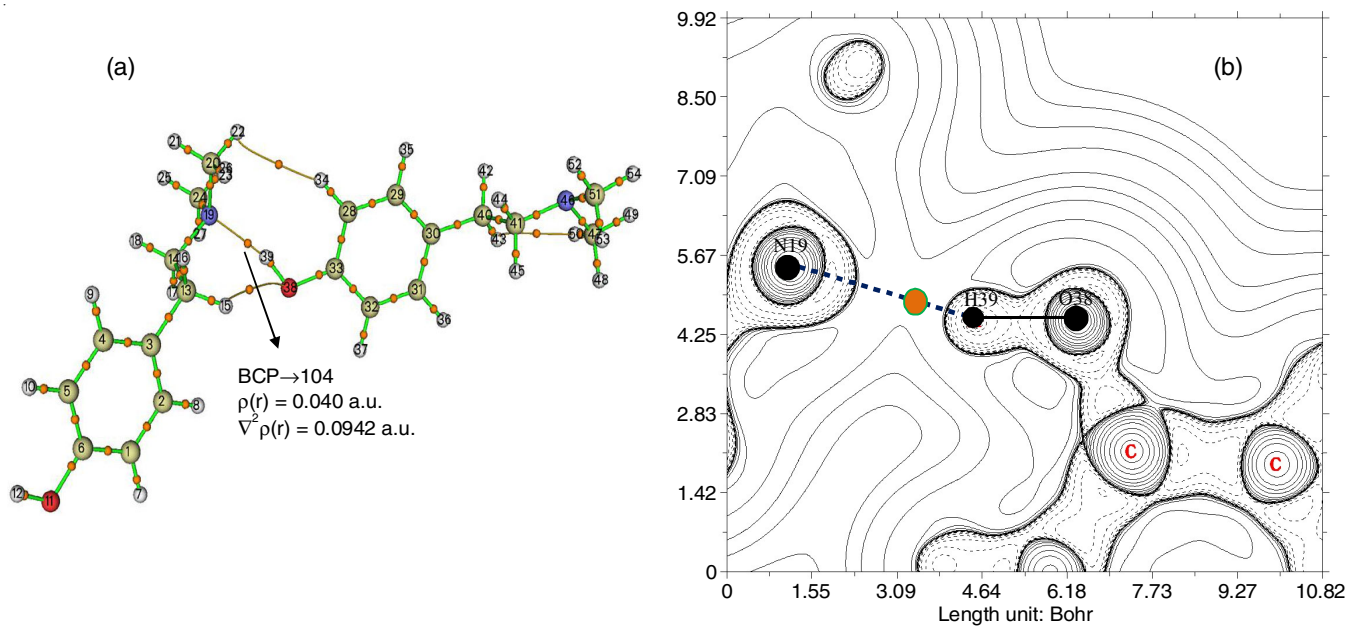

Fig. 14. Characterization of the O38–H39···N19 bond in D1 using AIM's topological parameters: (a) Molecular graph showing BCP, bond paths (BPs), $\rho(r_c)$ and $\nabla^2\rho(r_c)$ values; (b) Contour plot shows local charge concentration (dotted lines) and local charge depletion (solid lines); also are shown BP being indicated by the dotted blue line and orange dot by the BCP. The abscissa and ordinate scales are in Bohr units and the third axis of Laplacian values is not shown; All BCP, $\rho(r_c)$ and $\nabla^2\rho(r_c)$ values are presented in Table-13

TABLE-13
TOPOLOGICAL PROPERTIES OF THE ELECTRON DENSITY AND LAPLACIAN ELECTRON DENSITY COMPUTED AT ALL BCP's FOR ALL COVALENT BONDS IN THE D1 STRUCTURE OF HORDENINE (ALL VALUES ARE IN a.u.)

Bond path	BCPs[a]	$\rho(r)$[b]	$\nabla^2\rho(r)$[c]	Bond path	BCPs[a]	$\rho(r)$[b]	$\nabla^2\rho(r)$[c]
C1-C2	61	0.309	-0.859	C28-C29	102	0.306	-0.843
C1-C6	58	0.311	-0.882	C28-C33	97	0.308	-0.856
C2-C3	66	0.305	-0.836	C29-C30	99	0.306	-0.842
C3-C4	69	0.307	-0.845	C30-C31	92	0.305	-0.835
C3-C13	74	0.248	-0.579	C30-C40	95	0.248	-0.581
C4-C5	64	0.306	-0.842	C31-C32	86	0.309	-0.858
C5-C6	59	0.310	-0.867	C32-C33	91	0.309	-0.873
C1-H7	57	0.281	-0.964	C28-H34	107	0.278	-0.942
C2-H8	65	0.281	-0.965	C29-H35	108	0.279	-0.953
C4-H9	71	0.280	-0.957	C31-H36	82	0.279	-0.955
C5-H10	60	0.277	-0.935	C32-H37	81	0.28	-0.957
C6-O11	56	0.280	-0.370	C33-O38	93	0.289	-0.404
O11-H12	55	0.366	-0.025	O38-H39	98	0.331	-0.022
C13-C14	89	0.238	-0.531	C40-C41	87	0.238	-0.530
C13-H15	75	0.277	-0.927	C40-H42	101	0.275	-0.916
C13-H16	80	0.275	-0.916	C40-H43	96	0.275	-0.913
C14-H17	100	0.280	-0.955	C41-H44	78	0.279	-0.946
C14-H18	103	0.272	-0.892	C41-H45	72	0.269	-0.875
C14-N19	105	0.257	-0.651	C41-N46	79	0.265	-0.689
N19-C20	110	0.263	-0.678	N46-C47	77	0.268	-0.702
N19-C24	114	0.262	-0.673	N46-C51	73	0.268	-0.934
C20-H21	112	0.270	-0.884	C47-H48	70	0.267	-0.862
C20-H22	113	0.278	-0.938	C47-H49	76	0.277	-0.934
C20-H23	106	0.279	-0.950	C47-H50	83	0.278	-0.943
C24-H25	116	0.271	-0.889	C51-H52	68	0.277	-0.936
C24-H26	117	0.278	-0.940	C51-H53	62	0.267	-0.867
C24-H27	115	0.279	-0.947	C51-H54	67	0.277	-0.934
H43-H50	90	0.010	0.038	O38-H15	84	0.005	0.0217
H22-H34	111	0.003	0.012				

Note: [a]Bond critical points; [b] and [c]Refer to Electron density and Laplacian electron density for corresponding BCPs.

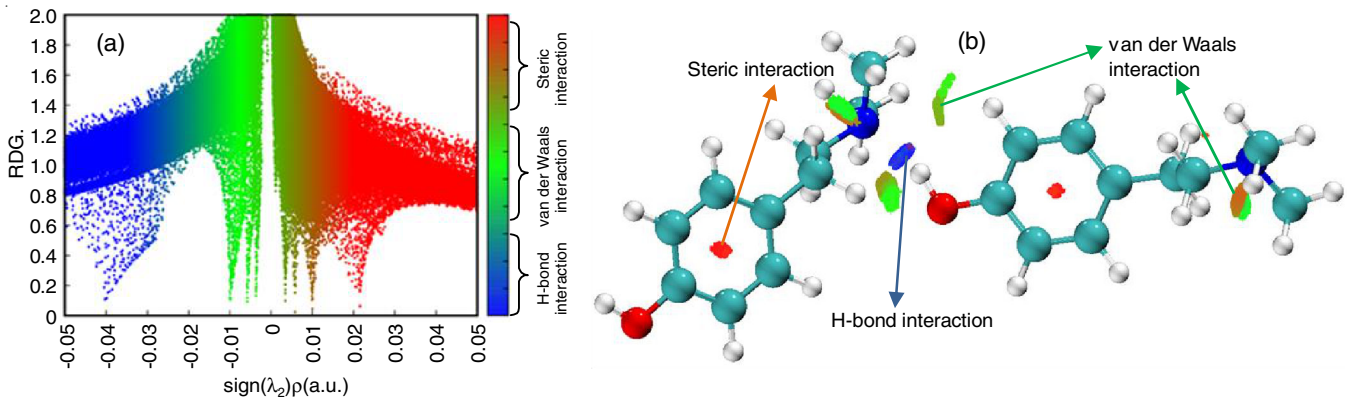

Fig. 15. (a) 2D scatter graph and (b) 3D visualization of RDG *versus* sign(λ_2)ρ(r) for D1 structure of hordenine (blue: H-bonding interaction, green: van der Waal interaction, red: steric interaction)

der Waals and steric clashes. The Johnson's NCI method of characterizing these three interactions in terms of the reduced density gradient (s) [44] was applied. Computed 's' values against the electron density $\rho(r_c)$ (where $\rho(r_c)$ values are multiplied with the algebraic sign of the eigen value λ_2) are plotted as 2D scatter graph (Fig. 15a). In order to discriminate the type of interactions colour codes are used [45]. An isosurface corresponding to a specific value of s in the form of 3D–visualization of the H–bond, van der Waals and steric interactions as shown in Fig. 15b. The blue isosurface between the O38–H39 bond and N19 atom shows the presence of the O38–H39···N19 bond. Similarly, inferences may be drawn in 2D scatter plot for RDG and sign(λ_2)$\rho(r_c)$ with value –0.04 a.u. corresponding to the intermolecular O–H···N bond. Further, the green isosurfaces extended from sign(λ_2)$\rho(r_c)$ from the value of 0.00 to –0.01 a.u.; it represents the van der Waals attraction between the monomers. In addition, the two troughs at the sign(λ_2)$\rho(r_c)$ values of 0.00 to 0.01a.u. (shaded green–orange isosurfaces in 3D) represent the hyperconjugative interactions for C14–H18···N19 and C51–H52···N46 bonds. The red surfaces in the monomer rings represent the steric interactions in the D1 structure.

Conclusion

A satisfactory intermolecularly –O–H···N bonded dimer model for hordenine has been proposed. The proposed dimer was selected out of many species computed from MD simulations followed by its optimization at B3LYP/6–311++G(d,p) level thereby yielding it as the most stable structure. The dimer has also shown O–H···O and C–H···N bonds. It has been shown that the O–H···O interaction is implicit and not observable either in XRD or in IR spectrum, the C–H···N bond interaction acts as a stabilizing factor in the overall dimer structure. Geometrical parameter characterization include determining the most stable dimer in agreement with the XRD structure in addition to the radius of gyration, minimum distances and root-mean-square deviations of the trajectories of the atoms in the dimer. Some degree of structural order within the dimer and between dimer species has been studied using the RDF. While the experimental vibrational IR and Raman spectral features fit satisfactorily with that due to the O–H···N bonded dimer, there are no observable spectral features attributable to the weak O–H···O and C–H···N bonds. The O–H···N and O–H···O bonds have been characterized using radial distribution function values in agreement with the geometrical criteria for H–bonds. A detailed analysis of the O–H···N and C–H···N bonds in terms of natural bond orbitals, electron densities and their Laplacian values and reduced density gradients has been presented. Molecular orbitals overlap description of the O–H···N, O–H···O and C–H···N bonds has shown that the O–H···N bond with the stabilization energy of S17.0 kcal/mol is a stronger H–bond interaction. This has been manifested in the bond paths of the three H–bonds corresponding to the BCP at (3, –1).

ACKNOWLEDGEMENTS

The authors thank the Director of USIC, Karnatak University for IR and Raman measurements performed under DST–funded PURSE Programme (Phse–I/II) analytical facilities. One of the authors, Jayashree J. Tonannavar is grateful to Prof. S. Umapathy at the Department of IPC, IISc, Bengaluru for a short–term visit to his laboratory for MD tutorials. Financial support received under the Center of Advanced Study–Phase–II Programme in the Department of Physics is acknowledged. The University Research Scholarship awarded to Jyoti Bhovi by Karnatak University is sincerely acknowledged.

CONFLICT OF INTEREST

The authors declare that there is no conflict of interests regarding the publication of this article.

REFERENCES

1. J. Ma, S. Wang, X. Huang, P. Geng, C. Wen, Y. Zhou, L. Yu and X. Wang, *J. Pharm. Biomed. Anal.*, **111**, 131 (2015); https://doi.org/10.1016/j.jpba.2015.03.032
2. S.C. Kim, J.H. Lee, M.H. Kim, J.A. Lee, Y.B. Kim, E. Jung, Y.S. Kim, J. Lee and D. Park, *Food Chem.*, **141**, 174 (2013); https://doi.org/10.1016/j.foodchem.2013.03.017
3. B.P. Mukhopadhyay, J.K. Dattagupta and M. Simonetta, *Z. Krist. New Cryst. Struct.*, **187**, 221 (1989); https://doi.org/10.1524/zkri.1989.187.14.221
4. M. Sobiech, J. Giebultowicz and P. Luliński, *J. Chromatogr. A*, **1613**, 460677 (2020); https://doi.org/10.1016/j.chroma.2019.460677
5. J.S. Fitzgerald, *Aust. J. Chem.*, **17**, 160 (1964); https://doi.org/10.1071/CH9640160

6. S. Anwar, T. Mohammad, A. Shamsi, A. Queen, S. Parveen, S. Luqman, G.M. Hasan, K.A. Alamry, N. Azum, A.M. Asiri and M.I. Hassan, *Biomedicines*, **8**, 119 (2020); https://doi.org/10.3390/biomedicines8050119
7. S. Ghose and J.K. Dattagupta, *Z. Kristallogr.*, **187**, 213 (1989); https://doi.org/10.1524/zkri.1989.187.3-4.213
8. C.J. Barwell, A.N. Basma, M.A.K. Lafi and L.D. Leake, *J. Pharm. Pharmacol.*, **41**, 421 (1989); https://doi.org/10.1111/j.2042-7158.1989.tb06492.x
9. A. Dwivedi, V. Dubey and A.K. Bajpai, *Int. J. Chem. Stud.*, **2**, 20 (2015).
10. M. Parvez and J.F. Malone, *Acta Cryst.*, **293C**, 1450 (1991); https://doi.org/10.1107/S0108270190012380
11. J. Priscilla, D.A. Dhas, I. Hubert-Joe and S. Balachandran, *J. Mol. Struct.*, **1229**, 129823 (2021); https://doi.org/10.1016/j.molstruc.2020.129823
12. R.F.W. Bader, *Chem. Rev*., **91**, 893 (1991); https://doi.org/10.1021/cr00005a013
13. M.J. Frisch, G.W. Trucks, H.B. Schlegel, G.E. Scuseria, M.A. Robb, J.R. Cheeseman, G. Scalmani, V. Barone, B. Mennucci, G.A. Petersson, H. Nakatsuji, M. Aricato, X. Li, H.P. Hratchian, A.F. Izmaylov, J. Bloino, G. Zheng, J.L. Sonnenberg, M. Hada, M. Ehara, K. Toyota, R. Fukuda, J. Hasegawa, M. Ishida, T. Nakajima, Y. Honda, O. Kitao, H. Nakai, T. Vreven Jr., J.A. Montgomery, J.E. Peralta, F. Ogliaro, M. Bearpark, J.J. Heyd, E. Brothers, K.N. Kudin, V.N. Staroverov, R. Kobayashi, J. Normand, K. Raghavachari, A. Rendell, J.C. Burant, S.S. Iyengar, J. Tomasi, M. Cossi, N. Rega, J.M. Millam, M. Klene, J.E. Knox, J.B. Cross, V. Bakken, C. Adamo, J. Jaramillo, R. Gomperts, R.E. Stratmann, O. Yazyev, A.J. Austin, R. Cammi, C. Pomelli, J.W. Ochterski, R.L. Martin, K. Morokuma, V.G. Zakrzewski, G.A. Voth, P. Salvador, J.J. Dannenberg, S. Dapprich, A.D. Daniels, Ö. Farkas, J.B. Foresman, J. Cioslowski, J.V. Ortiz and D.J. Fox, Gaussian 09, Revision A.1, Gaussian Inc., Wallingford CT (2009).
14. M.J. Abraham, D. van der Spoel, E. Lindahl, B. Hess, and the GROMACS development team, GROMACS User Manual version (2019); http://www.gromacs.org
15. J. Bhovi, J. Tonannavar and J.J. Tonannavar, *J. Mol. Struct.*, **1299**, 137077 (2024); https://doi.org/10.1016/j.molstruc.2023.137077
16. B. Hess, *J. Chem. Theory Comput.*, **4**, 116 (2008); https://doi.org/10.1021/ct700200b
17. W. Humphrey, A. Dalke and K. Schulten, *J. Mol. Graph.*, **33**, 7855, (1996); https://doi.org/10.1016/0263-7855(96)00018-5
18. T. Lu and F. Chen, *J. Comput. Chem.*, **33**, 580 (2012); https://doi.org/10.1002/jcc.22885
19. M.H. Jamróz, *Spectrochim. Acta A Mol. Biomol. Spectrosc.*, **114**, 220 (2013); https://doi.org/10.1016/j.saa.2013.05.096
20. L. Pallavi, J. Tonannavar and J. Tonannavar, *J. Mol. Liq.*, **352**, 118746 (2022); https://doi.org/10.1016/j.molliq.2022.118746
21. S. Zahn, K. Wendler, L. Delle Site and B. Kirchner, *Phys. Chem. Chem. Phys.*, **13**, 15083 (2011); https://doi.org/10.1039/c1cp20288j
22. Gromacs Manual-2023.3 Documentation, (2023); https://doi.org/10.5281/zenodo.7588711
23. A. Kantardjiev and P.M. Ivanov, *Entropy*, **22**, 1187 (2020); https://doi.org/10.3390/e22101187
24. D.H.D. Jong, L.V. Schäfer, A.H. De vries, S.J. Marrink, H.J.C. Berendsen and H. Grubmuller, *J. Comput. Chem.*, **32**, 1919 (2011); https://doi.org/10.1002/jcc.21776
25. A. Rakita, N. Nikolic, M. Mildner, J. Matiasek and A. Elbe-Bürger, *Sci. Rep.*, **10**, 1 (2020); https://doi.org/10.1038/s41598-019-56847-4
26. G.R. Desiraju and T. Steiner, The Weak Hydrogen Bond in Structural Chemistry and Biology, Oxford University Press: New York (1999).
27. G. Socrates, Infrared Characteristic Group Frequencies, John Wiley & Sons, New York, London, Sydney, Toronto (1980).
28. N.B. Colthup, L.H. Daly and S.E. Wiberley, Introduction to Infrared and Raman Spectroscopy, Academic Press Inc., New York and London (1964).
29. L.J. Bellamy, The Infrared Spectra of Complex Molecules, Chapman and Hall: London, edn. 3 (1975).
30. M.D. Prabhu, J.T. Yenagi, V. Kamat and J. Tonannavar, *J. Mol. Struct.*, **1218**, 128495 (2020); https://doi.org/10.1016/j.molstruc.2020.128495
31. D. Sajan, J. Binoy, B. Pradeep, K.V. Krishna, V.B. Kartha, I.H. Joe, V.S. Jayakumar, *Spectrochim. Acta A Mol. Biomol. Spectrosc*., **60**, 173 (2004); https://doi.org/10.1016/S1386-1425(03)00193-8
32. M. Karabacak, Z. Calisir, M. Kurt, E. Kose and A. Atac, *Spectrochim. Acta A Mol. Biomol. Spectrosc*., **153**, 754 (2016); https://doi.org/10.1016/j.saa.2015.09.007
33. J.P. Merrick, D. Moran and L. Radom, *J. Phys. Chem. A*, **111**, 11683 (2007); https://doi.org/10.1021/jp073974n
34. E.D. Glendening, C.R. Landis and F. Weinhold, *J. WIREs Comput. Mol. Sci.*, **2**, 1 (2012); https://doi.org/10.1002/wcms.51
35. V. Krishnakumar, D. Barathi, R. Mathammal, J. Balamani and N. Jayamani, *Spectrochim. Acta A Mol. Biomol. Spectrosc*., **121**, 245 (2014); https://doi.org/10.1016/j.saa.2013.10.068
36. S. Yalagi, J. Tonannavar and J. Tonannavar, *Heliyon*, **5**, e01933 (2019); https://doi.org/10.1016/j.heliyon.2019.e01933
37. S.S. Malaganvi, J.T. Yenagi and J. Tonannavar, *Heliyon*, **5**, e01586 (2019); https://doi.org/10.1016/j.heliyon.2019.e01586
38. L.F. Pacios, *J. Phys. Chem. A*, **108**, 1177 (2004); https://doi.org/10.1021/jp030978t
39. E. Espinosa, I. Alkorta, J. Elguero and E. Molins, *J. Chem. Phys.*, **117**, 5529 (2002); https://doi.org/10.1063/1.1501133
40. P.S.V. Kumar, V. Raghavendra and V. Subramanian, *J. Chem. Sci.*, **128**, 1527 (2016); https://doi.org/10.1007/s12039-016-1172-3
41. S.G. Aziz, A.O. Alyoubi, S.A. Elroby and R.H. Hilal, *Mol. Phys.*, **115**, 2565 (2017); https://doi.org/10.1080/00268976.2017.1335896
42. W. Zierkiewicz, J. Fanfrlík, P. Hobza, D. Michalska and T. Zeegers-Huyskens, *Theor. Chem. Acc.*, **135**, 217 (2016); https://doi.org/10.1007/s00214-016-1972-z
43. I. Rozas, I. Alkorta and J. Elguero, *J. Am. Chem. Soc.*, **122**, 11154 (2000); https://doi.org/10.1021/ja0017864
44. E.R. Johnson, S. Keinan, P. Mori-Sanchez, J. Contreras-García, A.J. Cohen and W. Yang, *J. Am. Chem. Soc.*, **132**, 6498 (2010); https://doi.org/10.1021/ja100936w
45. R. Laplaza, F. Peccati, R.A. Boto, C. Quan, A. Carbone, J.-P. Piquemal, Y. Maday and J. Contreras-García, *J. WIREs Comput. Mol. Sci.*, **11**, e1497 (2020); https://doi.org/10.1002/wcms.1497